Oxidation of Metals, Vol. 29, Nos. 1/2, 1988

The Influence of Ion-Implanted Yttrium on the Selective Oxidation of Chromium in Co–25 wt.% Cr

P. Y. Hou* and J. Stringer†

Received May 21, 1987

Specimens of Co-25 wt.% Cr, Co-25 wt.% Cr-1 wt.% Y, and yttrium-implanted Co-25 wt.% Cr alloy were oxidized at 1000°C in 1 atm O_2. The implantation dosage ranged between 10^{16} to 10^{18} ions/cm^2. The unimplanted binary alloy oxidized to a duplex Co-rich scale, but the Y-containing ternary alloy formed a continuous Cr_2O_3 layer. When the implantation dosages were lower than a nominal 10^{18} ions/cm^2, the alloy failed to develop a similar continuous Cr_2O_3 layer as that observed with the Y-containing alloy. A temporarily stable external Cr_2O_3 scale was formed on the most heavily implanted specimen (1×10^{18} Y^+/cm^2). This Cr_2O_3 scale consisted of very fine-grained oxide, which is permeable to the outward transport of Cr and Co. Internal oxidation pretreatment of the ion-implanted specimens converting the Y metal to its oxide prior to the oxidation experiment, can enhance the development of an external Cr_2O_3 scale, but this scale is also unstable. Results suggest that the selective oxidation of chromium in an ordinarily non-Cr_2O_3-forming alloy can be due to the reactive element oxides acting as preferential nucleation sites on the alloy surfaces, but the subsequent growth of these scales may require a continuous supply of reactive elements in the alloy.

KEY WORDS: Reactive element additions; ion implantation; selective chromium oxidation.

INTRODUCTION

One important effect of minor alloying additions of reactive elements or their oxides on Cr_2O_3-forming alloys is the selective oxidation of chromium.[1] This effect is particularly noticeable on alloy systems, which normally do

*Lawrence Berkeley Laboratory and Department of Materials Science and Mineral Engineering, University of California, Berkeley, California 94720.
†Electric Power Research Institute, Palo Alto, California 94303.

0030-770X/88/0200-0045$06.00/0

not have enough chromium to form a continuous external Cr_2O_3 scale. For this purpose, a dispersion of the reactive metal oxide is more effective than the corresponding reactive metals.[2] In Co-Cr alloy systems, protective Cr_2O_3 can be formed on alloys containing as low as 10 wt.% Cr with 1 wt.% Hf, Ti, or Zr internally oxidized prior to the oxidation.[2] Stringer and Wright[3] also observed the formation of a continuous Cr_2O_3 layer on Co-21 wt.% Cr with 3 vol.% Y_2O_3 addition, and Wright *et al.*[4] reported similar observations on a Co-13 wt.% Cr-3 vol.% Y_2O_3 alloy. In all cases, the dispersoid particles, whether mechanically added or internally formed in the alloy, were responsible for the selective oxidation of Cr to form a continuous Cr_2O_3 layer. This Cr_2O_3 layer developed across the entire specimen surface except at dispersion-free areas. Furthermore there was usually little overgrowth of the base metal oxides. In an alloy system that normally would develop the Cr_2O_3 protective scale upon oxidation, the reactive element addition reduces the time it takes to develop the continuous Cr_2O_3 layer, and there is again less base metal oxidation.

The ability of reactive metals or their oxides present in Cr_2O_3-forming alloys to promote the protective Cr_2O_3 scale development was first attributed by Davis *et al.*[5] to an enhanced chromium diffusion in the alloy. Studies[6,7] have shown that the diffusivity of chromium in a dispersion-containing (ThO_2 or CeO_2) Ni or Ni-Cr alloy was an order of magnitude higher than that of a dispersion-free alloy. Since the transition between external scale development and internal oxidation is dependent upon the interdiffusivity of the scale-corming species,[8] an increase in the diffusivity of chromium in the alloy (D_{Cr}^{alloy}) would naturally enhance the external Cr_2O_3 scale development.

Later diffusivity measurements carried out by Seltzer *et al.*[9,10] on Y_2O_3 and ThO_2 containing Ni-Cr and Co-Cr alloys have shown that the presence of dispersoids alone does not enhance the diffusivity of chromium in the alloy. However, D_{Cr}^{alloy} increases with decreased alloy grain sizes. When the alloy grain size of both the dispersion-containing and the dispersion-free alloys were the same, no enhanced D_{Cr}^{alloy} was observed. These results imply that any higher dislocation densities present in dispersion-containing alloys is not a major source for chromium diffusion in the alloy. Rather, grain-boundary diffusion dominates the overall chromium diffusivity. Their observations were in accord with those of Giggins and Pettit,[11] which showed that Cr_2O_3 developed on Ni-Cr alloys more readily over alloy grain boundaries than over the bulk of the grains, and on cold-worked surfaces, which recrystalize to form smaller grains, than on polished ones. Since both reactive metal and oxide dispersions tend to stabilize a fine alloy grain size,[12] the enhanced D_{Cr}^{alloy} observed earlier by Fleetwood[6] and Wenderott[7] can be explained as a result of the decreased grain sizes produced by the oxide

dispersions. Thus, it is possible that the presence of the reactive metals or oxides decreases alloy grain size, which in turn increases D_{Cr}^{alloy} and aids in the initial development of the Cr_2O_3 scale. Nevertheless, while Co-10 and 15 wt.% Cr alloys containing 1 wt.% Ti, Zr, or Hf failed to form even a continuous Cr_2O_3-healing layer, a continuous external Cr_2O_3 scale was promoted after an internal oxidation pretreatment converting the Ti, Zr, or Hf metal to its oxide.[2] There was no change in alloy grain size as a result of the internal oxidation, and it is equally unlikely that much substructure was generated by this treatment. This work indicates that the enhanced chromium diffusivity in the alloy caused by the decreased grain sizes cannot be a major factor in promoting the initial protective scale development. Rather, the evidence supports the mechanism suggested by Stringer *et al.*[13] that the oxide dispersions reduce spacings between the first formed nuclei on alloy surfaces and thus promote a continuous Cr_2O_3 scale.

The nucleation of Cr_2O_3 on a Ni-20Cr based alloy with or without the dispersion of Y_2O_3 was recently studied by Braski *et al.*[14] It was concluded that the earlier development of the protective Cr_2O_3 scale on dispersion-containing alloys could not be accounted for by the mechanism proposed by Stringer *et al.*,[13] since no preferential nucleation of any oxide particle was observed at dispersoid particles intersecting the specimen surface. The slight enhancement of Cr_2O_3 scale formation on dispersoid containing specimens were explained to be due to an increased flux of chromium to the specimen surface. This idea was supported by the fact that the dislocations in the fully annealed samples tend to be pinned by dispersoid particles and thus form easy diffusion channel for chromium. However, Braski *et al.*[14] also argued that this slight selective oxidation behavior in the very early stage could not have any significant overall effect on steady-state oxidation rates. Their results indicated that the major role of the dispersoids was not to cause the rapid formation of a continuous Cr_2O_3 film. Rather, it was to alter the microstructure of the scale which formed. The consequence of the modified microstructure was to make the scale less permeable to material transport.

Recently, ion implantation has been a technique widely used for the study of the reactive element effects. The technique permits incorporation of reactive metals into only the surface region of alloys. Subsequent oxidation behavior of the implanted alloys can then be compared with the untreated alloy or with alloys containing the reactive metals in the bulk. Among the group of Cr_2O_3-forming alloys, Ni-30Cr,[15,16] Ni-33Cr,[17] Fe-43Ni-43Ni-27Cr,[17] and a 20Cr-25Ni-niobium-stabilized austenitic stainless steel[18,19] have been used as the base alloys for the implantation studies. All these alloys are good Cr_2O formers; i.e., the alloys can develop a protective Cr_2O_3 external scale even without the presence of the reactive elements.

Although the implanted reactive elements, particularly Y and Ce, have been shown to reduce the transient stage of oxidation of these good Cr_2O_3 formers, it remains to be determined whether the presence of reactive elements on specimen surfaces alone could promote a continuous Cr_2O_3 scale formation on ordinarily non-Cr_2O_3 formers. The purpose of this study is to carry out such an evaluation.

The effect of different dosages of yttrium implant on the oxidation behavior of Co-25 wt.% Cr alloy has been studied at 1000°C in 1 atm O_2. Co-25 wt.% Cr is a borderline Cr_2O_3-former. At 1000°C in air, it oxidizes to form a Co-rich duplex structure.[20,21] But, with the reduction of the ambient p_{O_2} to less than 100 torr,[20] or with the inclusion of minor amounts of impurities such as Si,[22] it can oxidize to form a continuous external Cr_2O_3 layer. In order to compare the effect of reactive elements as implanted species or as alloying additions, the oxidation of a Co-25 wt%-1 wt.% Y alloy was also studied. Some of the implanted and some of the alloyed yttrium-containing materials were internally oxidized prior to the oxidation experiment, since reactive metal oxide dispensations have been shown[2] to be more effective in promoting Cr_2O_3 scale formation than the reactive metals themselves.

Experimental Procedure

Alloy Preparation

The CoCr binary alloy used in this study was prepared from high purity elements by induction melting and casting under an argon atmosphere. The alloy ingot was cleaned by machining off the outer surface layers and then was homogenized by annealing in evacuated, sealed quartz tubes for 24 hr at 1100°C. The grain size of the alloy ranged from 260 to 1040 μm, and the grains had an equiaxed structure free from inclusions.

The ternary CoCrY alloy with the nominal composition Co-25 wt.% Cr-1 wt.% Y was made from the binary CoCr alloy. A small portion of the homogenized Co-25Cr ingot was cut and placed with 99.9% pure Y chips in an alumina crucible and melted in an arc furnace under a reduced Ar atmosphere. The resulting ingot was a $25 \times 25 \times 19$-mm block. After machining off the outer layer of the ingot, it was homogenized at 1100°C in vacuum for 24 hr. X-ray diffraction analysis of this alloy did not show any Y-containing compounds except near the edges of the ingot, where Y_2O_3 was present due to some internal oxidation of the Y. Observation under the optical microscope showed that the Y concentrated at grain boundaries. The alloy grains were slightly elongated with a relatively uniform grain size. The average grain width was 28 μm and the average grain length was 61 μm. These grains were much smaller than those of the

Co-25Cr alloy. Results from chemical analysis showed that the actual Y concentration was 0.98 wt.%.

Ion Implantation

Ion implantation was carried out in the injector portion of the heavy ion linear accelerator (superHILAC) at the Lawrence Berkeley Laboratory. The acceleration voltage of the ions was usually adjusted to 400 keV, and the average current density was 3 μA/cm^2. Specimens used for the ion implantation were disc shaped, with a diameter of 15 mm and a thickness of 1 mm. Each specimen was polished to a 600-grit surface finish and carefully degreased immediately before the implantation. Individual specimens were held in an aluminum seat that covered 5 mm of the periphery of the specimen to give each specimen an implanted area next to an unimplanted area for later comparison of oxidation behaviors.

Dosages used in this study varied from 10^{16} to 10^{18} ions/cm^2. The desired dosage is a known function of the total amount of beam current to which the specimen is exposed. The actual dosage on the implanted face should, however, be less than that indicated by the total current because emission of secondary electrons from the specimen surface is not suppressed nor accounted for. Later experimental measurement of the implanted dosage on selected specimens using the Rutherford backscattering (RBS) technique showed that the error was about 50%. In this paper, a dosage is always referred to the value obtained from the total current, unless stated otherwise. It should be borne in mind that the actual dosage is only approximately half of this value. From estimates based on the theory proposed by Lindhard *et al.*,[23] the depth distribution of the ions can be calculated. The calculated maximum concentration and depth, together with the depth of the implanted zone are detailed in Table I. Results obtained from selected specimens

Table I. Distribution of Implanted Ions Using 400-keV Voltage

			Calculated by the LSS procedure			Experimental measurement by RBS			
Substrate	Ion implanted	Dosage (atoms/cm^2)	Max. consn. (at.%)	Depth (Å) of max. concn.	Depth (Å) of implant-ation	Dosage (atoms/cm^2)	Max. (concned (at.%)	Depth (Å) of max. concn.	Depth (Å) of implant-ation
Co-25Cr	Y^+	1×10^{16}	1.73	679	1478	3×10^{15}	0.45	605±60	1578
		5×10^{16}	8.63	679	1478	—	—	—	—
		3×10^{17}[a]	—	—	—	10^{16}–10^{17}	6.73	760±90	1595
		1×10^{18}	>100	679	1478	4×10^{17}	23.54	510±70	1430

[a]Implanted with three different voltages: 400, 800, and 1800 keV, with 1×10^{17} cm^2 dosage per voltage.

probed by backscattering with 2-MeV He ions are also presented in the same table.

Spatial distribution of the ions on the implanted surface is not very uniform, since the ion beam could not be rastered across the specimen surface. Since the beam intensity was the highest at the center of the beam, the variation in implanted dosage from edge to center in each specimen was found to be a factor of ~4. Occasionally, implanted specimens were annealed to remove radiation damage. The annealing was carried out in quartz tubes sealed under $\sim 1 \times 10^{-6}$ torr vacuum at 700°C for 5 hr.

Internal Oxidation Pretreatment

Internal oxidation of some ion-implanted Co–25Cr specimens was carried out prior to the normal oxidation experiments in order to convert the Y present in the alloy to Y_2O_3. Specimens of the untreated Co–25Cr alloy and of the Co–25–1Y alloy were always included during this pretreatment in order to make possible comparisons of their subsequent oxidation behaviors.

Equal weights of a $Cr–Cr_2O_3$ powder mixture were used to establish a p_{O_2}, which is high enough to oxidize the Y internally but not high enough to oxidize the Cr or Co in the alloy. The powder mixture and the specimens were put in separate arms of a dumbell-shaped quartz tube to avoid contact of the powders with the specimen surfaces. Since it is not desirable to clean the surfaces of the implanted specimens by subsequent polishing, precautions were made to minimize any possible contamination from the quartz by placing both the powder mixture and the specimens in separate alumina boats. Studies[24] had indicated that transition metals can react with vitreous quartz at high temperatures and liberate SiO gas, which can deposit on the specimen surfaces. The quartz tube containing the specimens and the powders were sealed under $\sim 10^{-6}$ torr vacuum. All internal oxidation runs were carried out at 1000°C. The ion-implanted specimens to be internally oxidized were pretreated for 2 hr. These specimens were only cleaned by washing in an ultrasonic bath of ethanol before the subsequent oxidation experiment.

Characterization of the specimens after the internal oxidation (IO) pretreatment was carried out using Auger analysis and secondary ion-mass spectrometry (SIMS). The IO treatment did not introduce a large amount of contaminants on the specimen surface, except some Si, which presumably came from the quartz tube the specimens were sealed in. The Si observed corresponded to Si associated with SiO_2. Not only was this Si present on the surface, it was also found penetrated into the alloy during the IO pretreatment. Continuous SIMS depth profiles of Y^+, YO^+, and O^- were determined on the implanted surfaces before and after IO pretreatment. The purpose of analyzing the YO^+ signal was to be sure that the implanted

yttrium had indeed been oxidized as a result of the IO process. Figure 1 shows the SIMS for Y^+, YO^+, and O^- on a 3×10^{17} Y^+-implanted specimen before and after IO pretreatment. It is seen that before the internal oxidation, both O^- and YO^+ were only present on the very surface of the specimen most likely due to oxidation of the surface Y from the atmosphere. After the internal oxidation, both profiles extended into the alloy, with the YO^+ profile closely resembling that of Y^+.

Oxidation

Oxidation tests were carried out in pure dry oxygen at 1 atm total pressure. A Cahn 2000 microbalance was used for kinetics measurements at 1000°C. Specimens were loaded into the apparatus and equilibrated with oxygen before the furnace was turned on. The heating rate of the quartz lamp radiation furnace was high enough to achieve a stable specimen temperature of 1000°C in 10 min. After the desired oxidation time, the furnace was turned off and specimens were cooled in O_2 to room temperature in ~30 min, during which time the weight lost due to any spallation could be measured on the microbalance.

Scale Characterization

Analyses of the oxidized specimens involved initial observations of the oxide top surfaces under a scanning electron microscope (SEM) equipped

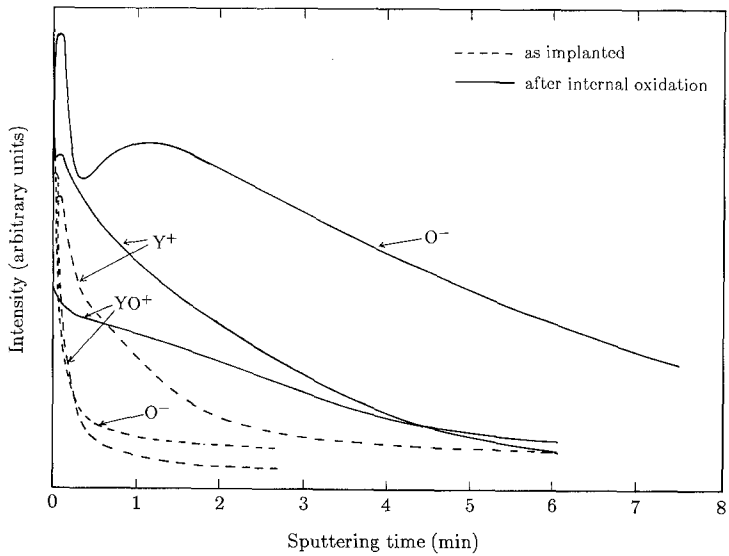

Fig. 1. Continuous SIMS depth profiles of Y^+, YO^+, and O^- on 1×10^{17} Y-implanted Co-25Cr before and after internal oxidation pretreatment. Sputtering was carried out using Ar with an approximate rate of 2500 nm/min.

with energy-dispersive X-ray analysis (EDX), while the oxides on selected specimens were examined by X-ray diffraction (XRD). Subsequently, these specimens were mounted and polished for cross-sectional observations using both an optical microscope and the EDX-equipped SEM. Some thin oxide scales were also studied using a Physical Electronics model 590 Scanning Auger Microprobe (SAM) and UTJ SIMS.

Results

Kinetics

On all implanted specimens, there was an appreciable amount of surface area that was shielded from the ion beam and therefore was not implanted The oxidation kinetics of the implanted surface needs to be corrected from the knowledge of the implanted area (A_1), the unimplanted area (A_2) and the weight gain behavior of the unimplanted specimens oxidized under the same condition. Thus

$$w_2 = \frac{\Delta w - w' A_1}{A_2}$$

where w_2 is the weight gain per unit area due to the implanted surface; Δw is the total weight gain from the implanted specimen; and w' is the average weight gain per unit area from the unimplanted specimen.

Figure 2 plots w_2 as a function of time for various ion-implanted Co-25Cr alloys oxidized under 1 atm O_2 at 1000°C. Annealing of the implanted specimens generally did not alter the oxidation kinetics. Also presented in Fig. 2 are the oxidation kinetics of the unimplanted Co-25Cr alloy and the yttrium-containing Co-25Cr-1Y alloy for comparisons. Perfect parabolic behavior was observed for the Co-25Cr-1Y and the $1 \times 10^{18}/\text{cm}^2$Y-implanted Co-25Cr specimens after the initial 5 hr of oxidation. The others only showed a near parabolic behavior after about 8 hr. Approximate parabolic rate constants were determined using $(\Delta m/A)^2 = f(t)$ linear plots. The constants are given in Table II, where the spallation behavior of these specimens is also described. From these results, strong dosage dependence was obvious. When the implanted Y^+ dosage was as high as 1×10^{18} ions/cm^2 (experimentally measured peak concentration equals 20–25 at.%), the growth rate became significantly reduced, and the scale was adherent. However, this slow growth behavior was only temporary. After longer oxidation times, the weight gain began to increase, as shown in Fig. 3, and the resulting scale again spalled upon cooling. Annealing this high dosage specimen had no effect on either the subsequent oxidation behavior or the adherence of the scale formed. Other implanted specimens showed progressively less effect in reducing the growth rate with less implanted dosages.

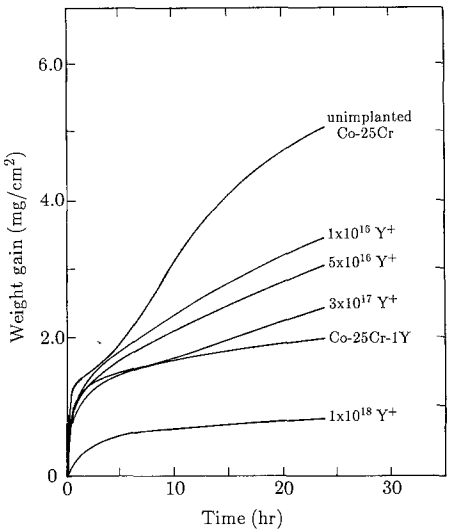

Fig. 2. Corrected weight gain-versus-time plot for various ion-implanted Co-25Cr alloys oxidized in 1 atm O_2 at 1000°C. The kinetics of unimplanted Co-25Cr and the yttrium bulk alloyed Co-25Cr-1Y are included for comparison. The implantation dosage is expressed in ions/cm^2.

Table II. Summary of Oxidation of Co-25Cr, Co-25Cr-1Y, and Co-25Cr (Ion-Implanted) Alloys after 24 hr in O_2 at 1000°C

Alloy	k_p ($mg^2\ cm^{-4}\ hr^{-1}$)	Spallation behavior
Co-25Cr	1.34 ± 0.21	General spallation detected after cooling
Co-25Cr-1Y	0.08	No spallation occurred.
Co-25Cr(La^{2+}, 1×10^{16})	0.49	Implanted area showed higher degree of spallation.
Co-25Cr(La^{2+}, 1×10^{16}) annealed	0.51	Implanted area spalled to the same degree as the unimplanted area.
Co-25Cr(Y^+, 1×10^{16})	0.44	Implanted area showed higher degree of spallation.
Co-25Cr(Y^+, 5×10^{16})	0.34	Implanted area showed higher degree of spallation.
Co-25Cr(Y^+, 3×10^{17})	0.26	Implanted area showed higher degree of spallation.
Co-25Cr(Y^+, 1×10^{18})	0.02	Implanted area showed no spallation.
Co-25Cr(Y^+, 1×10^{18}) annealed	0.02	Implanted area showed no spallation.

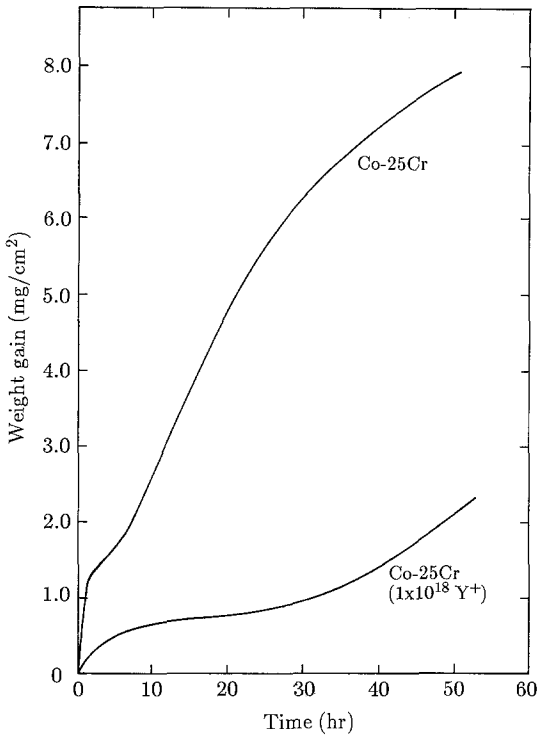

Fig. 3. Kinetics behavior of $1 \times 10^{18}/cm^2$ Y-implanted Co-25Cr after a longer oxidation time (50 hr) at 1000°C.

Furthermore, the scales formed on these implanted surfaces spalled more easily than that formed on the unimplanted surface. Annealing of these specimens did not alter the oxide growth behavior but eliminated the excess spallation tendency associated with the implantation.

Scale Morphology and Composition

The scales formed on the unimplanted Co-25Cr alloy under these oxidizing conditions are shown in Fig. 4. The oxidized Co-25Cr alloy developed a duplex structure with a ragged scale-alloy interface (Fig. 4a). Along the interface, there is a thin (2-6-μm), discontinuous Cr_2O_3 layer, as shown in the magnified scale in Fig. 4b. This layer was usually more complete in thinner scale regions. These thinner scales are referred to as Cr-rich protective scale in the remainder of this paper. They consisted mainly of three layers: a CoO layer decorated with Co_3O_4 at the scale-gas interface. a Cr_2O_3-healing layer at the scale-alloy interface, and a $CoCr_2O_4$

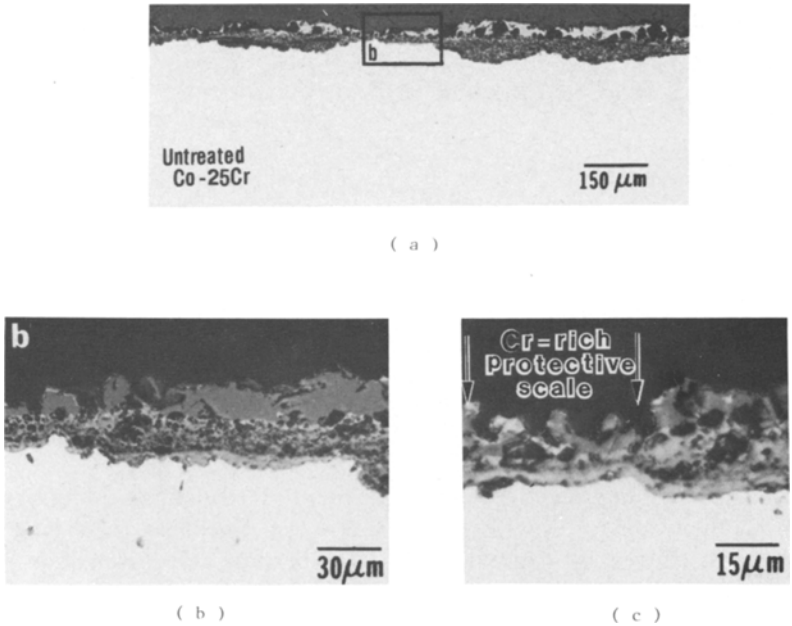

Fig. 4. Optical micrographs of the scale developed on the untreated Co-25Cr alloy. (a) General scale appearance after 24 hr at 1000°C in 1 atm O_2. (b) Magnified view from part of (a), showing areas with a more complete Cr_2O_3-healing layer at the scale/alloy interface. (c) Regions of protective thin scales.

spinel layer in between. This kind of structure, shown in Fig. 4c, is similar to that observed by Wright and Wood[21] on a Co-30Cr alloy. The fraction of surface covered by these Cr-rich protective scales was low on specimens oxidized for longer times (i.e., 24 hr, as the scale shown in Fig. 4a) but was much higher on specimens oxidized for only 3 hr.

Typical scale morphology developed on the Co-25Cr-1Y alloy after 24 hr at 1000°C is shown in Fig. 5. The scale consisted of a continuous inner layer of Cr_2O_3 and an outer layer of CoO mixed with Co_3O_4. Yttrium was internally oxidized at the front of the scale-alloy interface. Small particles were found on alloy grain boundaries, where the added yttrium had segregated before oxidation. The penetration depth of the internal oxidation zone was in general five times larger than the scale thickness.

With implantation dosages of less than $10^{18}/cm^2$, the scales formed showed little difference from that of an unimplanted specimen. There was generally a higher percentage of the Cr-rich protective scale on the implanted surfaces. This percentage increased with increasing implantation dosage. Figure 6 shows the scale formed on the 1×10^{16} Y-implanted Co–25Cr

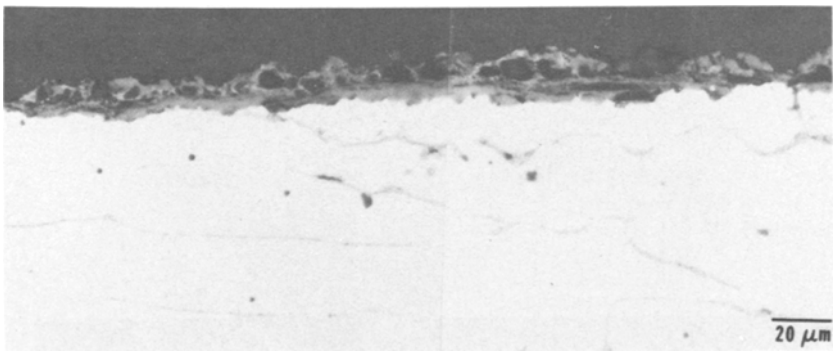

Fig. 5. Optical micrograph of the scale developed on the Co-25Cr-1Y alloy after 24 hr at 1000°C.

specimen. The thin protective scale as shown in Fig. 6a had a healing Cr_2O_3 layer at the scale to alloy interface of 2-6-μm thickness. This type of structure consisted of approximately 50% of the scale formed on the implanted surfaces. Other areas developed a Co-rich duplex scale, as shown in Fig. 6b,c. The thickness of these duplex scales varied noticeably. Some had a thin Cr_2O_3 healing layer near the alloy, some did not.

The scale developed on the more highly implanted specimen (3×10^{17} Y^+) is shown in Fig. 7. The scale was almost entirely the thin Cr-rich protective type with varying thickness (Fig. 7a). The Cr_2O_3-healing layer was found to be nearly continuous along the scale-alloy interface, except for a few locations, where the Co-rich duplex nodules were found. One of these large nodules is shown in Fig. 7b. Also shown in Fig. 7b are small fragments of what appears to be single-layered Cr_2O_3 scale. Indeed, SEM observation of scale top surfaces verified that on very rare and localized areas the oxide formed was only Cr_2O_3.

The scale morphology on the most heavily implanted Co-25Cr alloy (1×10^{18} Y^+) after 24 hr of oxidation is shown in Fig. 8. The unimplanted area showed the usual Co-rich oxide grains and large areas of spallation. The implanted side developed a fine-grained Cr_2O_3 scale, confirmed by XRD, with an average grain size <150 nm containing ~ 12 at.% Y, as detected using EDX. Most of the Y was present as Y_2O_3 after 4 hr of oxidation. Some had reacted to form $YCrO_3$, but the amount was comparatively small, as indicated by the relative intensities of YO^+ and $YCrO^+$ peaks in SIMS. With continued oxidation (after 24 hr), most of the Y was probably present as the chromite, since XRD of the scale scraped off the implanted surface showed faint lines corresponding to $YCrO_3$ only, not Y_2O_3. The Co content observed with EDX was primarily due to substrate contribution, since

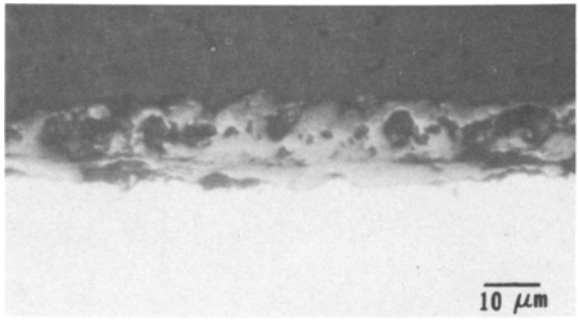

(a)

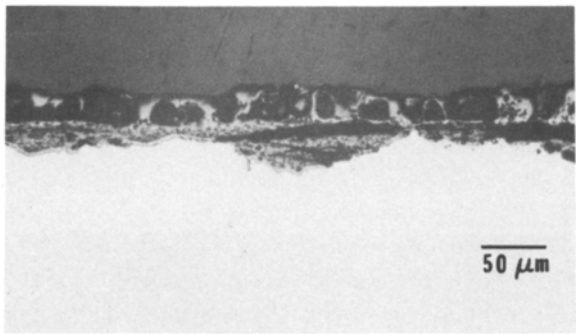

(b)

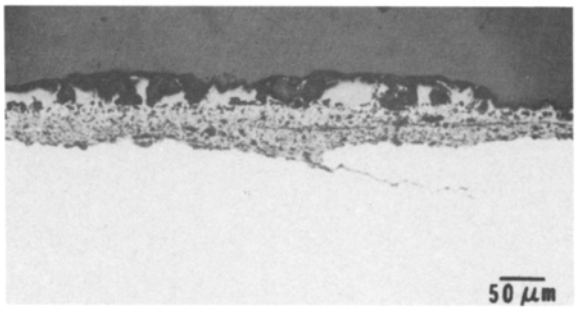

(c)

Fig. 6. Different scale morphologies observed on the 1×10^{16} Y-implanted Co–25Cr specimen after 24 hr at 1000°C. (a) Thin protective scale with a healing Cr_2O_3 layer. (b,c) Large nodular Co-rich scales.

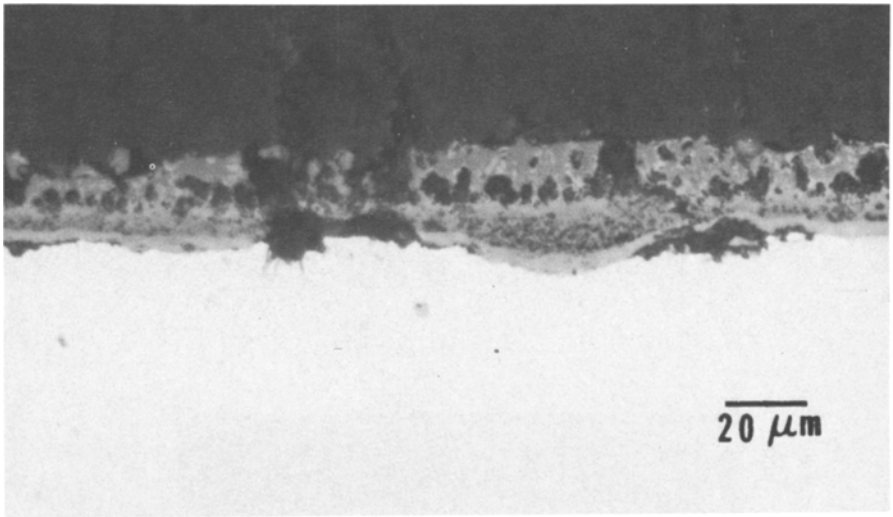

(a)

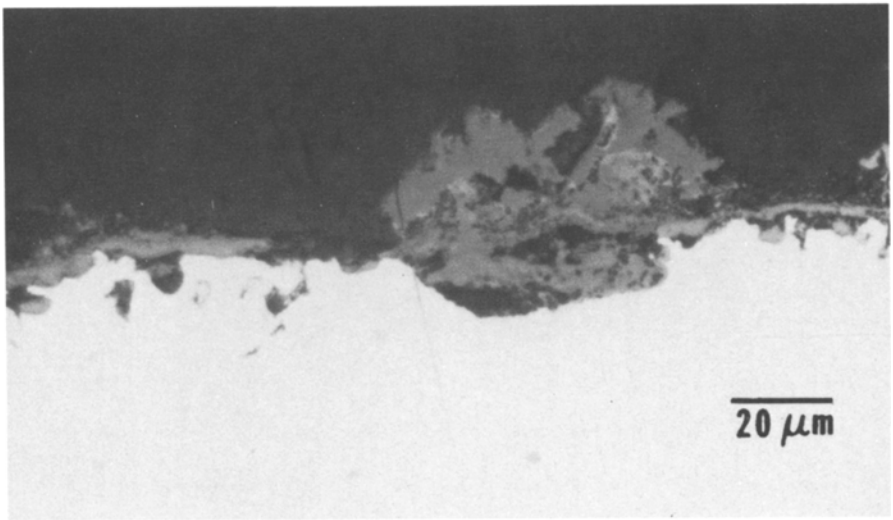

(b)

Fig. 7. Morphology of the scale formed on the 3×10^{17} Y-implanted Co-25Cr specimen after 24 hr at 1000°C. (a) Cr-rich protective type scale. (b) A large nodule growing through single-layer Cr_2O_3.

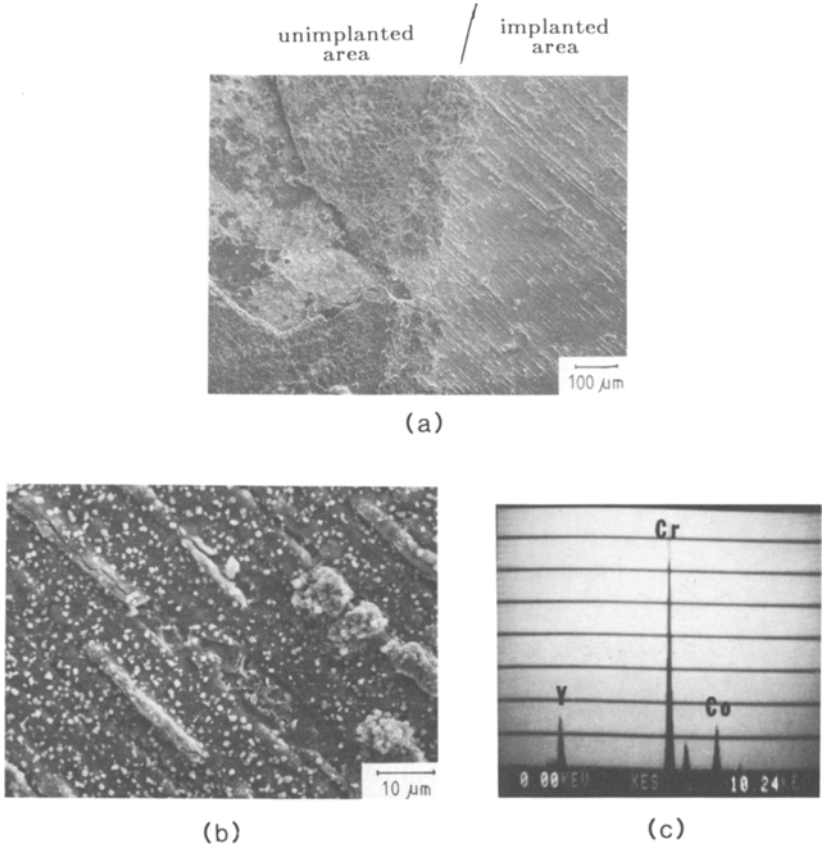

Fig. 8. Surface topography of 1×10^{18} Y-implanted Co–25Cr after 24 hr at 1000°C. (a) Interfacial area between implanted and unimplanted regions (b) Magnified view of the implanted region. (c) EDX of the scale formed on the implanted region.

only very little CoO phase was observed using XRD. Numerous individual Cr_2O_3 grains and Cr_2O_3 clusters can be seen growing out of the fine-grained oxide. Cracks were often found in these Cr_2O_3 clusters, and occasional spallation was observed. Examination of these spalled areas usually showed a number of pores near the scale-alloy interface.

Figure 9 shows a 40° tapered cross section of the scale. Comparison between scales formed near the unimplanted–implanted interface showed a dramatic difference between the scale morphologies. On the implanted side, the scale is seen to be single layered with occasional small nodules. The thin oxide has an approximate average thickness of 1.5 μm. Many individual Cr_2O_3 grains extending from the scale can be seen delineated

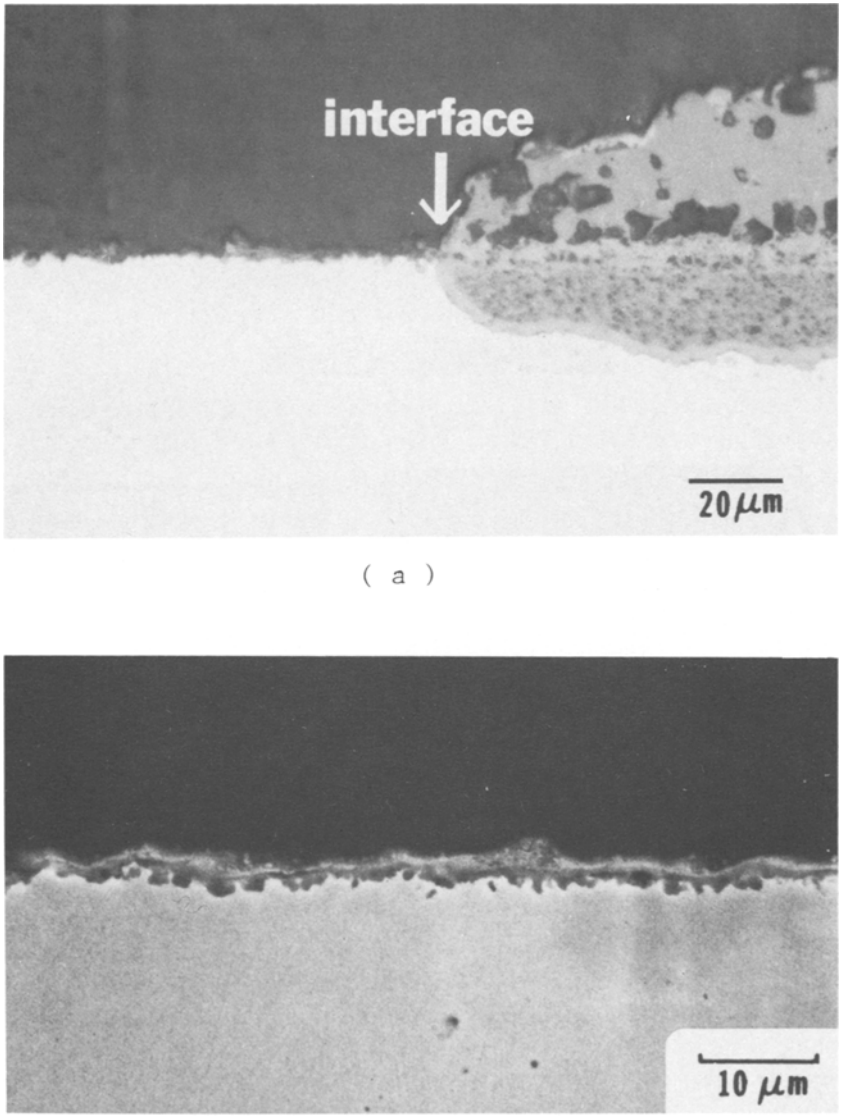

Fig. 9. Tapered cross section (40°) of the scale formed on the same specimen as that shown in Fig. 8. (a) Optical micrograph showing the implanted–unimplanted interface. (b) SEM image of the scale formed on the implanted region using back-scattered electrons.

within the alloy matrix. Large internal oxides of Cr_2O_3 were also abundant ahead of the scale.

In order to obtain a distribution profile of the Y in the scale, SIMS depth profiling was used and the result is shown in Fig. 10. The analysis was obtained from a 1×1-rastered area sputtered with high purity Ar. The sputtering rate was approximately 0.025 μm/min. Intensities of Cr, Y, and Co were measured at different intervals. Occasionally, the rastering mechanism was turned off for a very short period so that the intensities due to the center of the SIMS crater could be obtained. This method corrects for much of the cratering effect which leads to extended tailing. The curves drawn in Fig. 10 were corrected by this method. From the sputtering rate, the scale is calculated to be 1.4 μm thick. Y is no longer concentrated near the first 0.1 μm from the surface as in the case of the as-implanted specimen, but peaked about 0.5 μm away from the scale-gas interface. The scale formed behind the Y peak contained mainly Cr but before the Y peak, an appreciable amount of Co was detected.

When specimens with the highest dosage (1×10^{18} ions/cm^2) were oxidized for only 4 hr at 1000°C, extremely fine-grained oxide could be

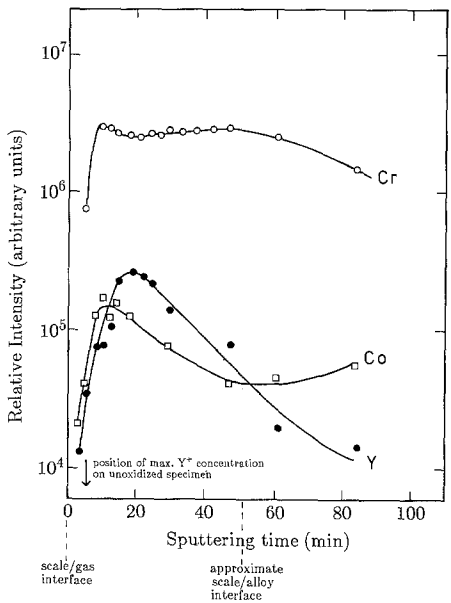

Fig. 10. SIMS depth profiles of Cr, Co, and Y through the scale formed on the same specimen as that shown in Fig. 8.

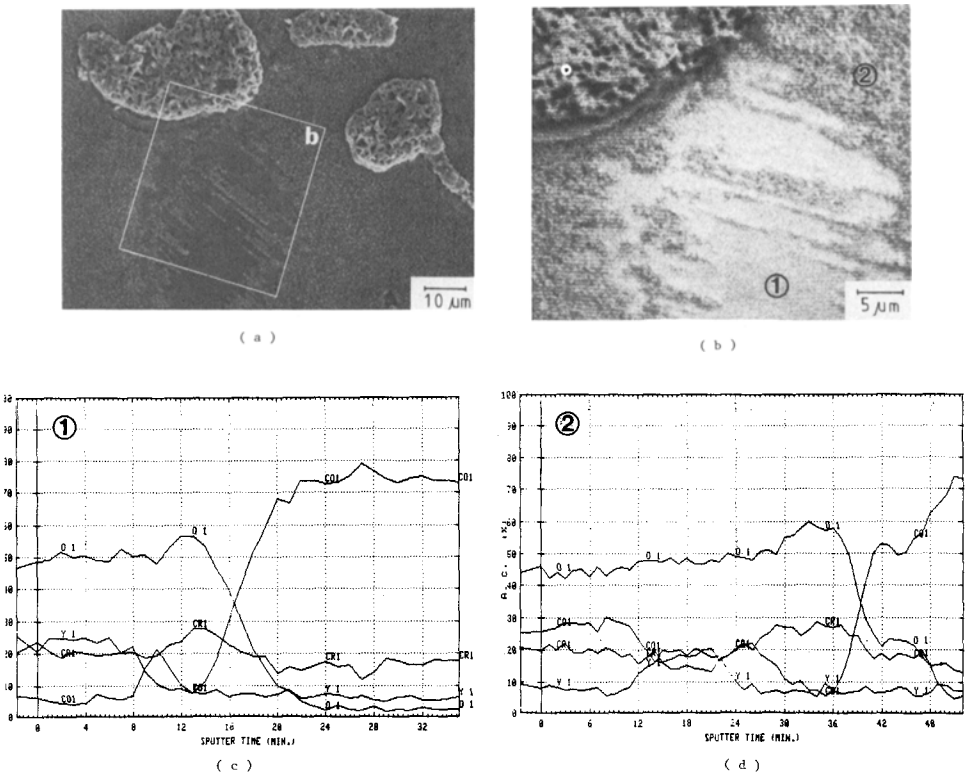

Fig. 11. (a) Surface oxides formed on Co–25Cr implanted with 1×10^{18} Y^+ after 4 hr of oxidation at 1000 °C. (b) Magnified area of (a) viewed with backscattered Auger electrons (c,d) Auger depth profiles of O, Cr, Co, and Y form points 1 and 2 marked in (b), respectively. The sputtering rate was approximately 2500 nm/min.

found on localized areas on the specimen surface. One of these areas is shown on the lower left-hand side of Fig. 11a. Again, Cr_2O_3 grains can be seen growing out of areas of this fine-grained scale. Occasionally, large nodular growths were also detected, as indicated by the three nodules shown. Figure 11b is a BSE image using Auger electrons. Areas that appeared brighter were richer in Y and were closely associated with the extremely fine-grained areas. Scanning Auger mapping of O, Y, Cr, and Co of this area also shows that the Y-rich region is totally free of cobalt but is heavily associated with oxygen. Figure 11c, d shows Auger depth profiles of points 1 and 2 marked on Fig. 11b respectively. The relatively high noise of the Auger peaks were due to charging of the oxide scale. It is seen that the very fine oxides were thin Cr_2O_3 layers with a Y profile unchanged from that of the as-implanted specimen indicating that the growth of this thin scale was totally due to oxygen inward diffusion. The scale thickness is 0.3–0.4 μm, about three times that of the original implantation depth. By contrast, the profile at point 2 showed an inward shift of Y as a consequence of the outward transport of Cr and Co through the originally developed thin scale and a scale more than twice as thick as that found at point 1 was observed. The scale composition detected at point 2 is very similar to the SIMS profile reported on scales formed after 24 hr of oxidation.

As indicated by kinetics studies, after oxidation of longer than 24 hr, the protective scale formed on the 1×10^{18} Y^+-implanted specimen started to break down. Figure 12a shows the implanted-unimplanted interface of the 1×10^{18} Y-implanted Co–25Cr specimen after 50 hr of oxidation. The scales formed on the implanted area now appeared similar to that on the unimplanted side and a great deal of spallation occurred. However, occasionally, small areas with the protective fine-grained Cr_2O_3 scale could still be found on the specimen surface mixed with large CoO grains, as shown in Fig. 12b.

Effect of Internal Oxidation Pretreatment

The effect of the internal oxidation treatment on the oxidation kinetics of Co–25Cr–1Y and 3×10^{17}Y-implanted Co-25Cr alloys is shown in Fig. 13. The kinetics curves obtained for the implanted specimens were again corrected from weight gains contributed by the unimplanted areas. The unimplanted specimen used for this correction was one that had received a similar internal oxidation treatment. It is important to use a Co–25Cr alloy treated with the same IO process, because the IO pretreatment reduces the oxidation rate of the Co–25Cr, as seen from approximate parabolic rate constants presented in Table III. The reduction in growth rate is probably due to the incorporation of Si into the alloy during the IO process. This behavior is similar to results reported by Jones and Stringer[22] that indicated

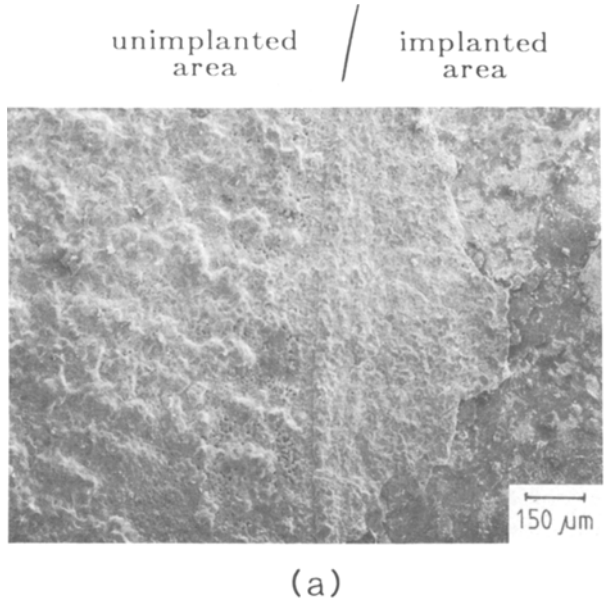

Fig. 12. Surface topography of scales formed on 1×10^{18} Y-implanted Co-25Cr after 50 hr of oxidation at 1000°C. (a) Interfacial area between implanted and unimplanted regions. (b) Magnified view of grains on the implanted region.

that the presence of Si associated with O in this alloy can significantly reduce its oxidation rate by promoting Cr_2O_3 scale formation.

From the results presented in Fig. 13 and Table III, it is seen that the internal oxidation treatment did not affect the overall oxidation behavior of the implanted Co-25Cr alloy, regardless of the implantation dosage. The scales formed after 24 hr of oxidation showed no apparent morphological differences between the IO-treated and untreated alloys. However, specimens implanted with the higher dosage showed a reduced initial oxidation rate, as shown in Fig. 14. This reduction is only temporary. After approximately 50 min, fast growth began and subsequent kinetics behavior resembled that of the non-IO-treated specimen. The scale that formed during the first hour of reduced oxidation was an adherent, continuous layer of Cr_2O_3, as shown in Fig. 15. This Cr_2O_3 scale consisted of a fine-grained ($<0.07\ \mu m$) layer on which larger-grained Cr_2O_3 clusters were scattered randomly. EDX analysis showed that yttrium is only detected with the fine-grained layer and some of the larger Cr_2O_3 clusters even contained cobalt. The thickness of this induced Cr_2O_3 layer was calculated to be $0.2\ \mu m$, assuming the scale was fully dense Cr_2O_3 with a density of $5.21\ g/cm^3$.[25] This thickness is comparable to the measured implantation depth, which is $\sim 0.17\ \mu m$.

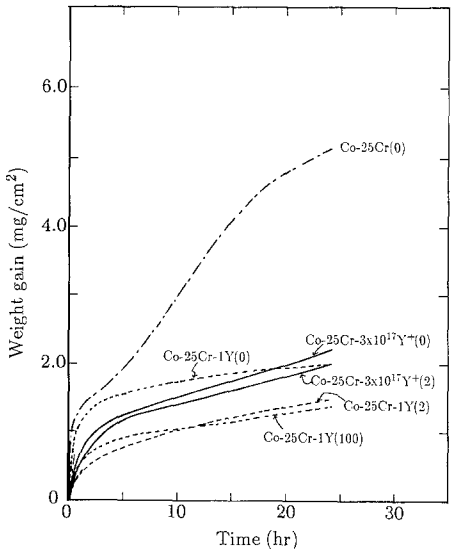

Fig. 13. Effect of internal oxidation pretreatment on the oxidation kinetics of Co-25Cr, Co-25Cr-1Y, and 3×10^{17} Y-implanted Co-25Cr. Numbers in parentheses indicate the duration of internal oxidation treatment in hours.

Table III. Parabolic Rate Constants of Internal Oxidation Treated Co-25Cr, Co-25Cr-1Y, and Co-25Cr(Y^+-Implanted) Alloys after Oxidation at 1000°C in O_2

Alloy	Duration of internal oxidation treatment at 1000°C (hr)	k_p ($mg^2\ cm^{-4}\ hr^{-1}$)	Spallation behavior
Co-25Cr	0	1.34 ± 0.21	Amount of spallation
Co-24Cr	2	0.49	decreased with decreasing
Co-25Cr	100	0.20	weight gain.
Co-25Cr-1Y	0	0.08	None of these showed
Co-25Cr-1Y	2	0.09	measurable spallation.
Co-25Cr-1Y	100	0.06	
Co-25Cr($1 \times 10^{16}\ Y^+/cm^2$)	0	0.44	All the implanted surfaces
Co-25Cr($1 \times 10^{16}\ Y^+/cm^2$)	2	0.46	showed slightly more
Co-25Cr($3 \times 10^{17}\ Y^+/cm^2$)	0	0.26	spallation than did
Co-25Cr($3 \times 10^{17}\ Y^+/cm^2$)	2	0.23	the untreated. Internal oxidation pretreatment renders no further effect.

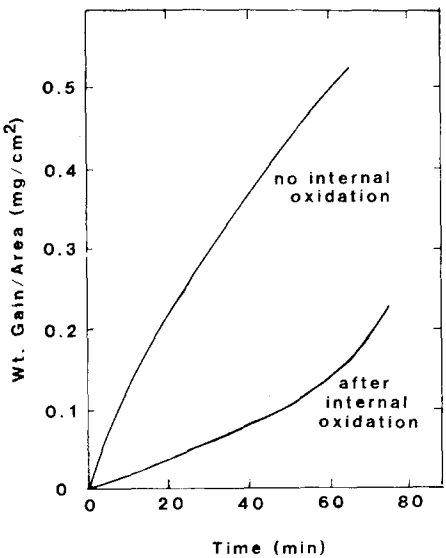

Fig. 14. Weight gain-versus-time behavior for the first hour of oxidation of the 3×10^{17} Y-implanted Co-25Cr specimen before and after the internal oxidation pretreatment.

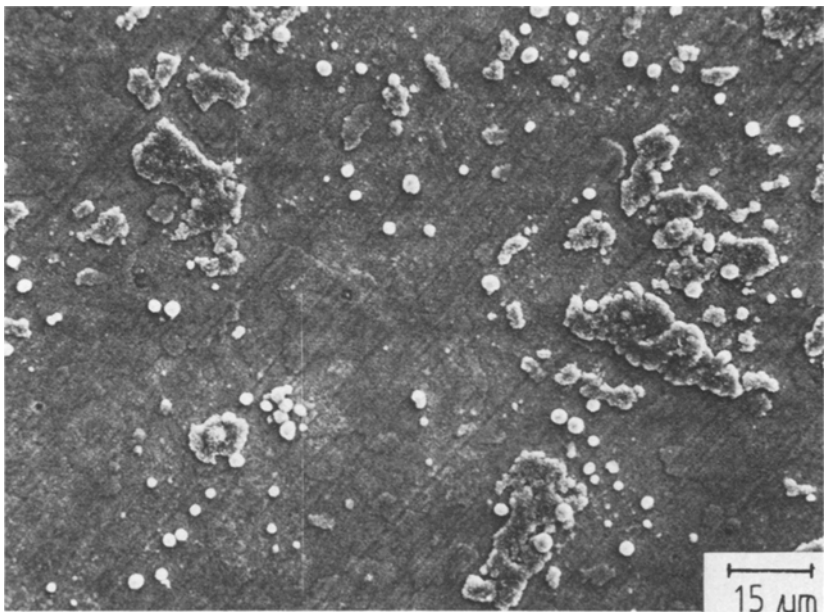

Fig. 15. Surface topography of the scale formed on the 3×10^{17} Y-implanted Co-25Cr after an internal oxidation pretreatment and 30 min of oxidation at 1000°C.

The effect of the internal oxidation treatment on the Co-25Cr-1Y was to reduce the initial stage of oxidation (see Fig. 13). The growth rate of the scale after the initial oxidation stage was unaltered from that of the untreated Co-25Cr-1Y alloy. Specimens treated with longer IO times which had a deeper IO zone did not show significant difference in the subsequent oxidation behavior from those treated with the shorter IO time. The scale that formed on IO-treated specimens contained mainly a continuous layer of Cr_2O_3, above which only a very thin layer of CoO is present at the scale/gas interface. These scales are also very adherent.

Discussion

The oxidation of the Co-25Cr-1Y alloy tested in this study showed the selective oxidation of Cr as expected. Initially, the oxidation rate was fast with the formation of a CoO-rich scale at the scale-gas interface. Subsequently, a continuous layer of Cr_2O_3 is developed under the Co-rich scale. Steady-state scale growth involves the thickening of this Cr_2O_3 layer, and the scale parabolic growth rate was nearly 17 times lower than that of the Co-25Cr alloy. After an internal oxidation pretreatment, the yttrium in the alloy is present as its oxide. These oxide particles were more effective in

reducing the transient stage of oxidation; giving rise to a much thinner outer CoO layer, and an earlier development of the continuous Cr_2O_3 scale.

The oxidation behavior of the Co-25Cr alloy after Y^+ ion implantation showed a strong dosage dependence. With an implantation dosage of 10^{16}-10^{17} ions/cm^2, which corresponds to an actual peak concentration of 2-7 at.%, the oxidation rate was reduced by a factor of 3-5. However, in no cases did the scale develop a continuous layer of protective Cr_2O_3 like that induced by the alloying addition of yttrium in Co-25Cr-1Y. With these lower dosages, the implanted specimens usually show a fast initial growth rate, sometimes even faster than that of the untreated alloy. Reduced steady-state growth is normally not observed until after about 2 hr of oxidation, by which time the weight gain of the specimen is already $\sim$1.2 mg/cm^2, which corresponds to metal removal far beyond the initial implantation depth of $<0.2\ \mu$m. Therefore, the subsequent reduction in scale growth rate must be associated with the implanted species being present in the scale and is not due to any modification of the initial scale development of the specimen. Metallographic observation of the scales formed on these implanted specimens showed that the scales are usually thinner than those formed without implantation. There is also a more continuous Cr_2O_3 healing layer at the scale-alloy interface. The area fraction of this Cr_2O_3 layer increases with increasing implantation dosage. But the development of this Cr_2O_3 layer is different from the selective oxidation of Cr associated with alloying additions of reactive elements. The major differences are that the Cr_2O_3 scale formed on the Y-containing alloy developed earlier, grew continuously as a complete layer, and showed no spallation upon cooling.

It is possible that in these cases, in which the scale formed is mainly cobalt oxides, the effect of implanted yttrium incorporated in the oxide scale is to retard Co^{2+} outward transport. The resultant reduction in the rate of CoO formation would then facilitate the development of the slower-growing but thermodynamically more stable Cr_2O_3 layer at the scale-alloy interface. The mechanism by which the Y_2O_3 particles retard Co^{2+} transport requires more detailed studies. Since all the implanted species in the scale are expected to concentrate in a relative narrow layer of about the thickness of the implantation depth, it is possible that this thin yttrium-modified layer may act as a barrier. This layer becomes more effective as the implantation dosage increases, thus showing the observed reduction in steady-state oxidation rate. Alternatively, Y_2O_3 particles may be concentrated at dislocations or grain boundaries in the scale and retard the transport of the diffusing species by these short-circuit diffusion paths.

The minimum implantation dosage that caused the formation of a continuous external Cr_2O_3 layer was a nominal 3×10^{17} Y^+/cm^2 after the

implanted Y had been converted to its oxide. If the implanted Y was present in its metallic form at the onset of oxidation, the amount of Y required to promote an external Cr_2O_3 layer is even higher: 1×10^{18} ions/cm^2. RBS analysis of the 3×10^{17} Y^+/cm^2-implanted specimen showed that the penetration depth of Y was ~0.16 μm, with a maximum concentration of 6.7 at.% at approximately 0.076 μm. The average concentration of Y within the implantation depth was therefore 3.5 at.%.

The fact that implanted reactive elements can indeed promote an external Cr_2O_3 scale with a much reduced grain size, and that an oxide dispersion of Y_2O_3 was more effective in promoting the external Cr_2O_3 scale than the implanted yttrium metal itself, all support the model proposed by Stringer *et al.*[13] that the reactive metal on the surface oxidizes to their oxide particles and act as preferential nucleation sites. Although the amount of implanted Y required for the selective oxidation of Cr is three to four times higher than with alloying additions, it is reasonable that a higher concentration is needed to act as nucleation sites in this case. Since there is no oxide dispersion beyond the immediate surface region of the implantation affected zone, the initially formed Cr_2O_3 nuclei cannot tolerate any undermining growth of the base metal oxide nuclei. Therefore, a higher concentration and thus a higher density of Cr_2O_3 nuclei are necessary for the development of a continuous protective scale before these individual nuclei are lifted away from the alloy surface by the fast-growing cobalt oxide.

Braski *et al.*[14] recently suggested that the model proposed by Stringer *et al.*[13] was not correct, as there was no observation of dispersoids acting as preferential nucleation sites. However, direct observation of Y_2O_3 acting as preferential nucleation sites may not be possible on a system in which the Y_2O_3 particles, with diameters of 5–100 μm, were uniformly distributed, while the earliest observation made was with a surface coverage of 40% or more of Cr_2O_3 with grain sizes ranging between 50–80 μm. The earlier development of a Cr_2O_3 scale on dispersion-containing alloys was explained to be a consequence of an increased chromium flux to the metal surface at the onset of oxidation. This increased chromium flux may be a result of a higher dislocation density beneath the alloy surface, as dislocations tend to be pinned to dispersoid particles. If this were indeed the case, one would expect any ion-implanted Cr_2O_3-forming alloy to show a selective oxidation of chromium, because the implantation process always causes enhanced diffusion through point defects or through an entangled dislocation network.[26] However, experimental results[15,17,19] have shown that none of the implanted inert gases (Ar[17] or Kr[27]) or implanted principal constituents of the alloys[15,19,27] was effective in reducing the transient stage of oxidation.

Although the initial development of external Cr_2O_3 scales on the Y-implanted surfaces may well be caused by the Y_2O_3 particles acting as

preferential nucleation sites, the inability of these scales to grow continuously is surprising. Normal oxide growth associated with the unimplanted binary alloy always starts after a short period of time. The length of this period is directly related to the implantation dosage. This breakdown behavior of the Cr_2O_3 scale is in contrast to the Cr_2O_3 scales formed on reactive element-containing alloys or even to the Cr_2O_3 scales developed on ion-implanted Cr_2O_3 formers, such as Ni-20Cr,[15] Ni-33Cr,[17] Fe-43Ni-27Cr,[17] and a 20Cr-25Ni-niobium-stabilized austenitic stainless steel.[18,19] For example, Bennett *et al.*[18] demonstrated that the Cr_2O_3 scales formed on Y- and Ce-implanted specimens were protective under cyclic oxidation conditions for up to 7000 hr. The highest implantation dosage used in their studies were 1×10^{17} ions/cm^2 which is comparable to the actual dosages used in this study. Therefore, the breakdown of the Cr_2O_3 scales found here could not have been caused by the incorporation of large amounts of Y_2O_3 or $YCrO_3$ particles in the oxide scales. The presence of these particles in the oxide scale, particularly at grain boundaries, has been suggested to reduce the oxide scale plasticity,[28] which may lead to easier oxide cracking. Furthermore, of all the Cr_2O_3 scales formed on reactive element-implanted Cr_2O_3-forming alloys, the implanted species were incorporated within the Cr_2O_3 scales.[15-19] This incorporation often occurs at the very early stage of oxidation.[16,19] In other words, in the systems in which the Cr_2O_3 scale is continuously protective, there is also a lack of yttrium supply in the alloy soon after a continuous Cr_2O_3 external layer is development. Thus, the breakdown of the Cr_2O_3 scale formed on the Y-implanted, non-Cr_2O_3-forming alloy in this study could not be accounted for by either (1) a lack of yttrium in the alloy to act as vacancy sinks,[29,30] or (2) a lack of yttrium in the alloy to trap impurities from diffusing to the scale-alloy interface.[31,32]

Examination of the initially formed Cr_2O_3 scale indicated that the scale first grew by inward transport of oxygen, giving rise to an extremely fine-grained Cr_2O_3 layer, which was very adherent. However, subsequent growth involved outward transport of Cr as well as Co through localized areas on the initially formed Cr_2O_3 layer. This process produced clusters of larger-grained oxides which were less adherent, and a number of interfacial voids could be found at the base of these clusters. The loss of scale adhesion at this point seems to be associated with the change in scale growth direction. This continued outward growth process leads to the final breakdown of the initially promoted Cr_2O_3 layer. It is not clear why there should be a change in the scale growth mechanism; i.e., scale growth shifted from predominantly oxygen inward transport to predominantly cation outward transport. However, it is known that this shift occurs at a very early stage: soon after the oxide thickness exceeded the initial implantation depth. As suggested by the study of Braski *et al.*,[14] the major role of reactive metal oxides in

the alloy is to alter the microstructure of the Cr_2O_3 scale formed, making it less permeable to material transport. It is possible that the Cr_2O_3 scale developed on the Y^+-implanted surfaces may have a different microstructure than that formed on a Y-containing alloy, making the scale more permeable to the outward transport of Cr and Co. If this were indeed the case, the difference in microstructures could not have been caused by any radiation effects associated with the implantation process. This is because annealed or internal oxidation pretreated specimens also develop unstable scales that broke down in a similar manner as those grown on as-implanted specimens. Further investigation is needed to elucidate the reason for the instability of these Cr_2O_3 scales, and thus the cause for their breakdown at temperatures.

CONCLUSIONS

The Y-containing Co–25 wt.% Cr–1 wt.% Y alloy oxidized to form a continuous and adherent Cr_2O_3 layer after an initial stage, during which time fast-growing cobalt oxide developed. After an internal oxidation pretreatment, converting the Y metal to its oxide, the transient stage of oxidation was reduced, resulting in an earlier development of the Cr_2O_3 scale with little cobalt oxide formation.

The influence of ion-implanted yttrium on the oxidation behavior of Co–25 wt.% Cr alloy can be summarized as follows:

1. With the actual implantation dosage of 3×10^{15} to 10^{16} ions/cm^2, the initial stage of oxidation was not affected. The oxide scale developed after 24 hr of oxidation at 1000 °C showed a duplex structure with a noncontinuous Cr_2O_3 healing layer at the scale–alloy interface. This structure is similar to the oxide developed on the unimplanted alloy, except that the area fraction of the Cr_2O_3-healing layer is higher. This area fraction increased with increasing implantation dosage. Scales formed on these implanted surfaces showed a higher degree of spallation than those formed on the unimplanted surfaces. However, this excessive spallation behavior could be eliminated if the implanted specimen had been thermally annealed prior to the oxidation tests.
2. The concentration of implanted yttrium needed to induce selective chromium oxidation was higher than if the yttrium were present as alloying additions. In this study, the minimum implantation dosage required for the development of a continuous external Cr_2O_3 scale was found to be 4×10^{17} ions/cm^2, as measured by RBS.
3. Oxide dispersions of the reactive element are more effective in promoting the Cr_2O_3 scale than the reactive metal itself. This was

demonstrated on a Y^+-implanted specimen after an internal oxidation pretreatment converting the yttrium metal to its oxide. The minimum implantation dosage needed for the selective chromium oxidation in this case dropped to 10^{16}-10^{17} ions/cm^2.

4. The Cr_2O_3 scale promoted by the presence of the implanted species had a very small grain size and was very adherent. It initially grew by oxygen inward transport, but subsequent growth involved outward transport of Cr and Co through localized areas. This outward growth process produced clusters of larger-grained oxides that were less adherent, and a number of interfacial voids were present at the base of these clusters.
5. The external Cr_2O_3 scales formed on the implanted surfaces failed to remain protective under oxidizing conditions. Normal oxide growth associated with the unimplanted Co-25 wt.% Cr alloy began after a short period of time. The length of this period is related to the implantation dosage. The higher the dose, the longer was the period before normal growth was observed. The thickest Cr_2O_3 scale found in this study was only about 1.5 μm before its breakdown.

ACKNOWLEDGMENTS

This work was supported by the Electric Power Research Institute under contract No. RP2261-1, through an agreement with the director, Office of Energy research, Office of Basic Energy Sciences, Materials Sciences Division of the U.S. Department of Energy under contract DE-AC03-76SF00098.

REFERENCES

1. D. P. Whittle and J. Stringer, *Philos. Trans. R. Soc. Lond.* **A27(56)**, 309 (1979).
2. D. P. Whittle, M. E. El Dahshan, and J. Stringer, *Corros. Sci.* **17**, 879 (1977).
3. J. Stringer and I. G. Wright, *Oxid. Met.* **5**, 59 (1972).
4. I. G. Wright, B. A. Wilcox, and R. I. Jaffee, Final Report on Naval Air Systems Command Contract No. WOO 19-72-C-0190, January 1983.
5. H. H. Davis, H. C. Graham, and I. A. Kvernes, *Oxid. Metal.* **3**, 431 (1971).
6. M. J. Fleetwood, *J. Inst. Met.* **94**, 218 (1966).
7. B. Wenderott, *Z. Metallk.* **56**, 63 (1965).
8. C. Wagner, *Z. Elektrochem.* **63**, 772 (1959).
9. M. S. Seltzer, B. A. Wilcox, and J. Stringer, *Met. Trans.* **3**, 2391 (1972).
10. M. S. Seltzer, *Met. Trans.* **3**, 2357 (1972).
11. C. S. Giggins and F. S. Pettit, *Trans. TMS-TIME* **245**, 2509 (1969).
12. P. Nannai, C. T. H. Stoddart, and E. D. Hondros, *Mat. Chem.* **1**, 297 (1976).
13. J. Stringer, B. A. Wilcox, and R. I. Jaffee, *Oxid. Met.* **5**, 11 (1972).
14. D. A. Braski, P. D. Goodell, J. V. Cathcart, and R. H. Kane, *Oxid. Met.* **25**, 29 (1986).
15. F. H. Stott, J. S. Punni, G. C. Wood, and G. Dearnaley, Conference Proceedings on *Transport in Non-stochiometric Compounds* (Pennsylvania State University, 1984).

16. C. H. Yang, G. E. Welsch, and T. E. Mitchell, *Mat. Sci. Eng.* **69**, 351 (1985).
17. J. Pivin, C. Roques-Carmes, J. Chaumont, and H. Bernas, *Corros. Sci.* **20**, 947 (1980).
18. M. J. Bennett, G. Dearnaley, M. R. Houlton, and R. W. M. Hawes, *Ion Implantation into Metals* (Pergamon, New York, 1981), p. 264.
19. M. J. Bennett, B. A. Bellamy, C. F. Knights, and Nicola Meadows, *Mat. Sci. Eng.* **69**, 359 (1985).
20. P. K. Kofstad and A. Z. Hed, *J. Electrochem. Soc.* **116**, 1542 (1969).
21. I. G. Wright and G. C. Wood, *Oxid. Met.* **11**, 163 (1977).
22. D. E. Jones and J. Stringer, *Oxid. Met.* **9**, 409 (1975).
23. J. Lindhard, M. Scharff, and H. E. Schiott, *Mat-Fys. Medd. K. Dan. Vidensk. Selsk.* **33**, 14 (1963).
24. R. Brueckner, *J. Non-Cryst. Solids* **5(2)**, 123 (1970); **5(3)**, 177 (1970-1971).
25. G. V. Samson (ed.), *The Oxide Handbook*, 2nd ed., IFI/Plenum, New York, 1982.
26. G. Dearnaley, J. H. Freeman, R. S. Nelson, and J. Stephen, *Ion Implantation* (North-Holland, Amsterdam, 1973).
27. J. E. Antill, M. J. Bennett, R. F. A. Carney, G. Dearnaley, F. H. Fern, P. D. Goode, G. L. Myatt, J. F. Turnaer, and J. B. Warburton, *Corros. Sci.* **10**, 729 (1976).
28. J. D. Kuenzly and D. L. Douglass, *Oxid. Met.* **8**, 139 (1974).
29. J. Stringer, *Met. Rev.* **11**, 113 (1966).
30. J. K. Tien and F. S. Pettit, *Met. Trans.* **3**, 1587 (1972).
31. A. W. Fundenbusch, J. G. Smeggil, and N. S. Bornstein, *Met. Trans.* **16A**, 1164 (1985).
32. J. G. Smeggil, A. W. Funkenbusch, and N. S. Bornstein, *Met. Trans.* **17A**, 923 (1986).